

Regional variability in dust-on-snow processes and impacts in the Upper Colorado River Basin

S. McKenzie Skiles,^{1*} Thomas H. Painter,¹ Jayne Belnap,² Lacey Holland,³ Richard L. Reynolds,⁴ Harland L. Goldstein⁴ and John Lin³

¹ Jet Propulsion Laboratory, California Institute of Technology, Pasadena, CA, USA

² Southwest Biological Science Center, U.S. Geological Survey, Moab, UT, USA

³ Department of Atmospheric Science, University of Utah, Salt Lake City, UT, USA

⁴ Geosciences and Environmental Change Science Center, U.S. Geological Survey, Denver, CO, USA

Abstract:

Dust deposition onto mountain snow cover in the Upper Colorado River Basin frequently occurs in the spring when wind speeds and dust emission peaks on the nearby Colorado Plateau. Dust loading has increased since the intensive settlement in the western USA in the mid 1880s. The effects of dust-on-snow have been well studied at Senator Beck Basin Study Area (SBBSA) in the San Juan Mountains, CO, the first high-altitude area of contact for predominantly southwesterly winds transporting dust from the southern Colorado Plateau. To capture variability in dust transport from the broader Colorado Plateau and dust deposition across a larger area of the Colorado River water sources, an additional study plot was established in 2009 on Grand Mesa, 150 km to the north of SBBSA in west central, CO. Here, we compare the 4-year (2010–2013) dust source, deposition, and radiative forcing records at Grand Mesa Study Plot (GMSP) and Swamp Angel Study Plot (SASP), SBBSA's subalpine study plot. The study plots have similar site elevations/environments and differ mainly in the amount of dust deposited and ensuing impacts. At SASP, end of year dust concentrations ranged from 0.83 mg g⁻¹ to 4.80 mg g⁻¹, and daily mean spring dust radiative forcing ranged from 50–65 W m⁻², advancing melt by 24–49 days. At GMSP, which received 1.0 mg g⁻¹ less dust per season on average, spring radiative forcings of 32–50 W m⁻² advanced melt by 15–30 days. Remote sensing imagery showed that observed dust events were frequently associated with dust emission from the southern Colorado Plateau. Dust from these sources generally passed south of GMSP, and back trajectory footprints modelled for observed dust events were commonly more westerly and northerly for GMSP relative to SASP. These factors suggest that although the southern Colorado Plateau contains important dust sources, dust contributions from other dust sources contribute to dust loading in this region, and likely account for the majority of dust loading at GMSP. Copyright © 2015 John Wiley & Sons, Ltd.

KEY WORDS snow energy balance; snowmelt; dust-on-snow; light absorbing impurities; snow hydrology; spatial variability

Received 22 September 2014; Accepted 1 June 2015

INTRODUCTION

The semi-arid Colorado Plateau region of the western United States is an erosional landscape that is one of the main dust producers in North America, along with the Great Basin, Mojave, and Sonoran deserts (Reynolds *et al.*, 2001; Reynolds *et al.*, 2003; Neff *et al.*, 2008). Biological and physical soil crusts stabilize the soils in many places in this region, but mechanical disturbance of these surfaces, from activities such as grazing, oil, and gas development, and off-highway vehicles decreases threshold frictional velocity below typically observed wind speeds, making sediments more available for transport (Belnap and Gillette, 1998). Beginning with the distur-

bance of the western US by Anglo settlement in the mid-19th century, the mountain snow cover of the Colorado River Basin (CRB) has been subject to five-fold or greater dust loading from this region (Neff *et al.*, 2008), rates which appear to be increasing over the last 15 years (Brahney *et al.*, 2013).

When deposited at the snow surface, dust accelerates snowmelt through albedo feedbacks: the darkening of the snow surface directly reduces albedo, and this indirectly reduces albedo by accelerating the growth of snow effective grain size. This dust-induced snow albedo feedback advances melt, shifts timing, and intensity of peak runoff and reduces total water yield (Painter *et al.*, 2010; Skiles *et al.*, 2012; Deems *et al.*, 2013). Recent research indicates that neglecting dust-on-snow processes may be a factor contributing to operational river-runoff-forecast errors in the CRB (Bryant *et al.*, 2013). This situation has important hydrologic implications in a

*Correspondence to: S. McKenzie Skiles, Jet Propulsion Laboratory, California Institute of Technology, 4800 Oak Grove Drive, Pasadena, CA 91109, USA.
E-mail: skiles@jpl.nasa.gov

region where mountain snow melt contributes over 70% of flow to the Colorado River, a heavily allocated waterway that provides water to seven states of the US and Mexico (Christensen *et al.*, 2004; Hamlet *et al.*, 2005).

Here, we expand upon previous work presented in Painter *et al.* (2012) and Skiles *et al.* (2012), studies that together assessed interannual variability in energy balance, dust loading/radiative forcing, and snowmelt runoff between 2005 and 2010 using energy-balance fluxes and snow measurements from two study areas in a single basin (Senator Beck Basin Study Area; SBBSA) in the San Juan Mountains (SJM) of southwestern CO, USA. The SJM are the first high-altitude area of contact for predominantly southwesterly winds transporting dust from the semi-arid landscapes of the southern Colorado Plateau/Four Corners region (where Utah, Arizona, Colorado, and New Mexico intersect), making SBBSA an ideal location to study the impacts of dust deposition to mountain snow cover. The majority of dust-deposition events at SBBSA are observed during spring (March–June), coinciding with peak wind speeds, dust emission, and atmospheric dust loading during these months (Lawrence *et al.*, 2010; Painter *et al.*, 2012; Flagg *et al.*, 2013; Sorooshian *et al.*, 2013). These events are also the most effective at initiating snow albedo feedbacks, as they coincide with increasing solar irradiance and onset of snowmelt (Painter *et al.*, 2012).

Multiple strands of evidence point to the source region for dust-on-snow in the CRB as the Colorado Plateau physiographic region. These include particle size and isotopic analysis of deposited dust to remote sensing imagery of discrete source dust plumes and back-trajectory analysis (Painter *et al.*, 2007; Neff *et al.*, 2008; Lawrence *et al.*, 2010; Neff *et al.*, 2013). Also, dust radiative forcing, retrieved from the Moderate Resolution Imaging Spectroradiometer (MODIS) using the Dust Radiative Forcing in Snow model (MODDRFS), exhibits a decreasing regional gradient moving northeast from the southern Colorado Plateau source region, with radiative forcing being highest in the SJM (Painter *et al.*, 2012).

Although we know dust-on-snow deposition is widespread in the upper CRB from observations and remote sensing imagery, SBBSA has been, until recently, the only study area with the necessary instrumentation to facilitate modelling and understanding of the impacts of dust-on-snow. A third snow energy balance site, Grand Mesa Study Plot (GMSP), located to the north of the SJM, was installed in 2009. Remote sensing images of dust emission events from the southern Colorado Plateau showed that dust was typically transported to the south of Grand Mesa, and the site location was selected specifically to capture regional variability in dust source, dust loading, and snowmelt response. In this paper, we assess the variability in dust-on-snow processes by

comparing the 4-year (2010–2013) dust source, deposition, radiative forcing, and snowmelt modelling record at Grand Mesa with the San Juan Mountain record over the same time period.

PREVIOUS WORK

The understanding of impacts from dust-on-snow in the upper CRB has increased with detailed study of processes at two well-instrumented study plots in SBBSA in southwestern CO. The SBBSA was established to study and monitor the hydrologic impacts of dust-on-snow, and instrumentation suites were installed to capture the necessary measurements to assess snow energy balance fluxes (latent and sensible heating/net solar and longwave radiation) to improve measurement and modelling of dust-on-snow processes. Descriptions of the study area, instrumentation, and data record can be found in Painter *et al.* (2012) and Landry *et al.* (2014).

Painter *et al.* (2007) utilized the first 2 years of data from SBBSA to isolate the effects of dust from other controls and showed that the acceleration of melt by the shortwave radiative forcing of dust resulted in a loss of snow cover in this region by about a month. Skiles *et al.* (2012) expanded this analysis to assess the interannual variability in dust loading, radiative forcing, and snowmelt rates over a 6-year record (2005–2010); mean springtime dust radiative forcing across the period ranged from 31 to 75 W m⁻² shortening snow cover duration by 21 to 51 days. The dust-advanced loss of snow cover was found to be linearly related to total dust concentration at the end of snow cover, despite temporal variability in dust exposure and solar irradiance. The advanced melt due to dust resulted in faster and earlier peak snowmelt outflow compared with relatively dust-free snow conditions, with daily mean snowpack outflow doubling under the heaviest dust conditions. This study also compared the relative capacity of dust and warmer temperatures to advance melt and found dust efficacy to be greater: increases of 2–4 °C advanced melt by 5–18 days in the absence of dust and 0–6 days in the presence of dust.

METHODS

Study areas and instrumentation

The relative location of the study areas and their location within the CRB are shown in Figure 1. GMSP is located in an opening in a pine forest on the northern rim of the Grand Mesa in west central Colorado at 3239 m. Swamp Angel Study Plot (SASP) is located in the lower part of SBBSA, in a clearing below tree line in a subalpine forest at 3368 m, making it only slightly higher

DUST-ON-SNOW SPATIAL VARIABILITY

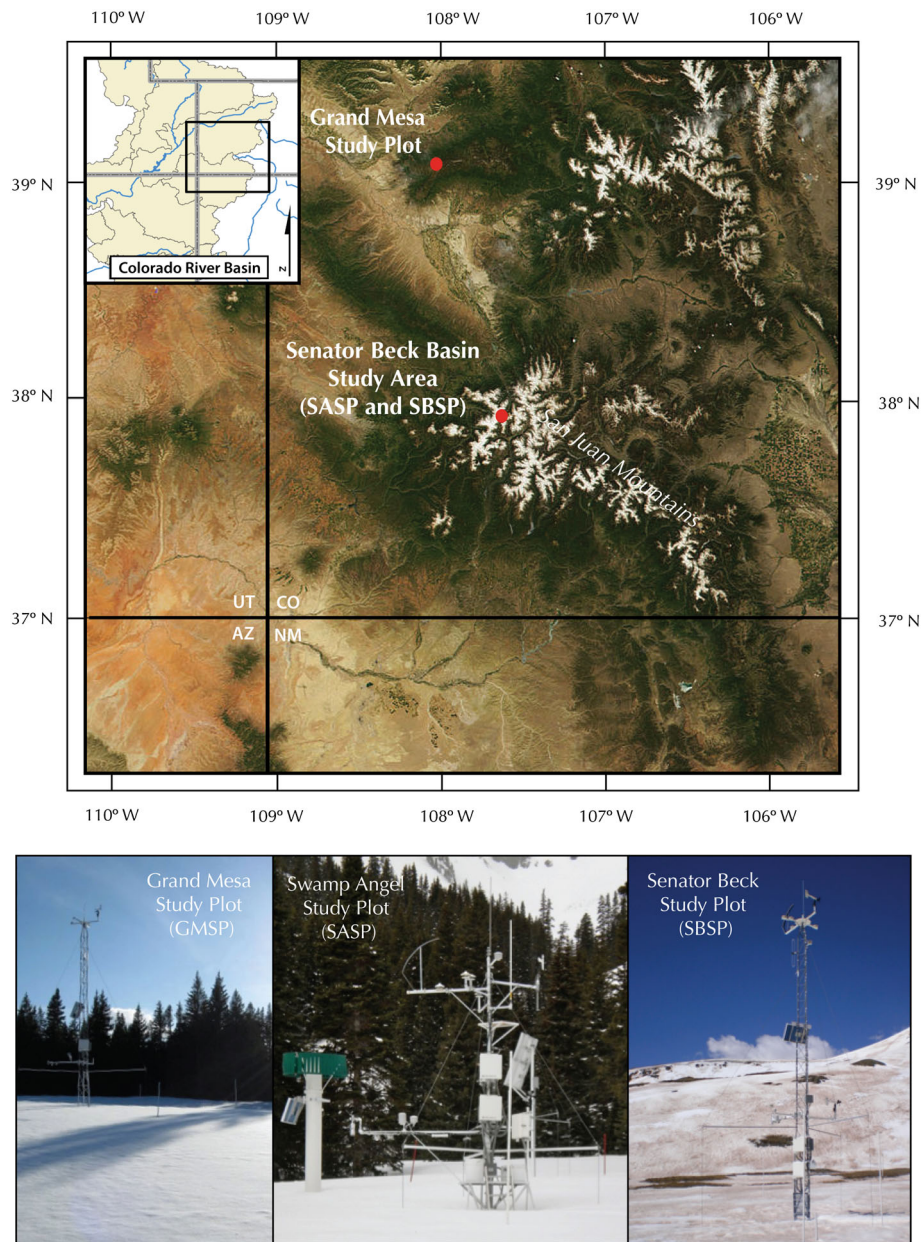


Figure 1. (A) Map of study areas, inset indicates location of study areas within the Colorado River Basin. (B) Photographs of instrumentation towers and study plots

in elevation (129 m) than GMSP. In this analysis, we mainly focus on SASP and GMSP, given their similar site elevations and environments. The additional study plot in SBBSA, Senator Beck Study Plot (SBSP), is located in the alpine tundra (3719 m) above tree line, at a level site near the centre of SBBSA. We include results from the alpine SBSP site in the advanced snowmelt section only, to highlight the similar response to dust radiative forcing at all three sites.

All three sites consist of a snow profile plot that contains a tower holding the instrumentation array. Tower measurements include wind speed and direction (at two

heights), air temperature and relative humidity (at two heights), snowpack depth, incoming and outgoing broadband (BB; 0.285–2.800 μm) and near-infrared/shortwave-infrared (NIR/SWIR; 0.695–2.800 μm) solar radiation, and incoming longwave radiation values. Incoming and outgoing visible solar radiation is calculated as the difference between the broadband and NIR/SWIR (VIS; 0.285–0.695 μm). Outgoing longwave radiation is inferred from measurement of snow surface temperature from an infrared sensor. Reflected radiation measured at the towers is corrected for slope and aspect via a hexagonal array of vertical snow depth measurement

stakes deployed around the tower (Painter *et al.*, 2012). Study plots and instrumentation arrays are pictured in Figure 1. Precipitation is measured only at SASP. Precipitation at SBSP is inferred from that at SASP. Precipitation at GMSP is from the nearby 'Mesa Lakes' Snow Telemetry site (SNOTEL; NRCS), which is located approximately 500 m north of GMSP at 3048 m under the assumption that precipitation is similar at the two sites.

Dust observations and snow sampling

Since 2003, the presence of airborne dust and subsequent deposition in snow at SBBSA have been visually identified as dust events and recorded by Center for Snow and Avalanche Studies (CSAS) observers. After each event, surface collections of dust loading, referred to as bulk samples, were made by sampling the snow in a shallow layer over a 0.5 m² area. These samples were melted and sent to the Geosciences and Environmental Change Science Center of the United States Geological Survey (USGS) in Denver, CO, USA, where snow was evaporated from samples, dust was dried and preserved for composition and particle-size analysis, and dust loading was reported grams of dust per metre squared of snow (g m⁻²). There are currently three full seasons (2011–2013) that have a consistent per-event dust loading record at SASP. This count excludes dust layers that were deposited on dust already at the surface, as these cannot be uniquely sampled. This dataset is made available through the CSAS (www.snowstudies.org). Since 2009, the detection of coincident dust events and source regions has been investigated by the USGS using remote sensing imagery and time-lapse photography, datasets that are currently available through 2012 (http://sgst.wr.usgs.gov/dust_detection/dust-events/).

In addition to specific dust-event snow sampling, the snowpack at SBBSA is monitored through regular excavation of snow pits to the ground. Sampling intervals were once a month, while snowpack was accumulating, increasing to weekly intervals beginning no later than April 15th, which is the average date of peak snow water equivalent (SWE). Weekly measurements begin earlier after significant dust deposition occurred. Snow sampling was most frequent at SASP, the easiest site to access. Measurements in the snow pits include: temperature profile, snowpack stratigraphy, liquid water content, and measurements of snow density. SWE, the amount of water that is held within the snowpack, was calculated from depth and density measurements. Dust stratigraphy was measured and quantified in the top 30 cm of the snow column at 3-cm intervals for a total of 10 samples, with accurate sample volumes maintained by use of a gravimetric board. The sampling depth of 30 cm is the approximate maximum depth to which dust and other

light absorbing impurities can influence radiative forcing. Snow samples were sent to the Snow Optics Laboratory at NASA's Jet Propulsion Laboratory (SOL/JPL), where they were filtered and weighed to find dust concentration in mg g⁻¹ of melted sample, which is equivalent to parts per thousand by weight (pptw).

The distance between SBBSA and GMSP inhibits regular observations at the latter, more northern site. Snow is sampled at GMSP at minimum once a month beginning in March by either CSAS or SOL/JPL. Note that in 2013, the final collection of the year was a bulk sample for dust loading and not a gravimetric sample for dust concentrations, although we were able to estimate dust concentration from this sample. The temporal resolution of sampling does not typically allow for individual dust event collections, but otherwise snow sampling and observations are identical to that described for SBBSA.

Modelling

Dust-source region. Dust sources on the Colorado Plateau and across the western US are dispersed. Therefore, we chose back-trajectories footprints over vectors to investigate source-regions for the two sites. These footprints were produced for each observed spring dust event (after 1 March) with the Stochastic Time-Inverted Lagrangian Transport (STILT) model (Lin *et al.*, 2003). Conceptually, footprints are considered as changes in concentration at the receptor site that can be attributed to different upwind source areas along the back-trajectories. In this interpretation, the footprints indicate the sensitivity in concentrations at the receptor site to surface fluxes along the back-trajectories for each modelled grid cell and time (units of ppm/($\mu\text{mole m}^{-2} \text{s}^{-1}$)⁻¹). Further discussion of the derivation of footprints can be found in Lin *et al.* (2003).

As a Lagrangian particle dispersion model, STILT uses an air parcel-following coordinate system, which offers distinct numerical and computational advantages over fixed-coordinate Eulerian models. Among these advantages are robustness against numerical diffusion, increased computational efficiency, and improved representation of atmospheric boundary layer transport effects (Lin, 2012). STILT calculates back-trajectories from wind fields produced by a different gridded meteorological model. These back-trajectories represent the paths of air parcels (i.e. fictitious particles) followed over the course of the simulation to arrive at a receptor site (location of interest) at the time the simulation was initialized.

The STILT simulations here were driven with meteorological fields from the Eta Data Assimilation System at 40-km horizontal resolution with an initial release of 3000 particles at a height of 30 m above ground level over each

receptor site. Three thousand particles were released every 6 h for the duration of each event. Back-trajectories out to -24 h were produced for each release. The -24 h time period was selected because the sites are in close proximity to the source regions in northeastern Arizona and northwestern New Mexico, and emission and deposition events were consistently observed on the same day. Footprints were derived for each release on a $1/6^\circ$ latitude and $1/4^\circ$ longitude horizontal grid, over which the particle-number densities were time-integrated for each grid-cell volume. Multiple six-hourly releases were then averaged to produce a footprint representative for the duration of the event. These simulations were run without the explicit consideration of a settling velocity to account for dust loading within the back-trajectory model, such that the spatial extent of footprints may be overestimated.

Radiative forcing. The range of potential radiative forcing due to dust is estimated using the treatment described in Painter *et al.* (2007). Briefly, to bracket the potential dust impact, radiative forcing is calculated using two scenarios. The minimum scenario addresses the first direct effect of dust in snow by accounting for the reduction in visible albedo. The maximum scenario addresses both the first direct effect as well as the first indirect effect by accounting for reduction in visible albedo due to dust and changes in grain size.

Minimum surface radiative forcing F_{dmin} (W m^{-2}) is calculated as

$$F_{dmin} = E_{vis}\Delta_{vis} \quad (1)$$

where E_{VIS} is the visible irradiance (W m^{-2}), $\Delta_{vis} = 0.92 - \alpha_{vis}$, α_{vis} is calculated visible albedo (from tower measurements) and 0.92 is the mean visible albedo for dust-free snow.

Maximum surface radiative forcing $F_{dmax+i1}$ is calculated as

$$F_{dmax+i1} = 0.5(E_{vis}\Delta_{vis} + E_{nir}\alpha_{nir}((1/\zeta) - 1)) \quad (2)$$

where if

$$\Delta_{vis} \leq 0.17 \text{ then } \zeta = 1 - 1.689\Delta_{vis}$$

else if,

$$\Delta_{vis} > 0.17 \text{ then } \zeta = 0.67$$

where the subscript '+i1' indicates that this accounts for the first indirect effect, E_{nir} is the NIR/SWIR net shortwave flux, and α_{nir} is the NIR/SWIR albedo. The latter relationship gives the proportion of the change in NIR/SWIR albedo due to the presence of dust versus grain coarsening in the absence of dust, and was developed from measurements at SBBSA (Painter *et al.*, 2007). This

method is useful because the record is continuous and does not require manual snow observations.

Radiative forcing from the Painter method was validated with direct estimates of radiative forcing from measurements of snow density, optical grain size, and dust concentrations using the SNow, ICe, and Aerosol Radiation (SNICAR; offline version 8d) model (Flanner and Zender, 2005; Flanner *et al.*, 2007) across 32 days between 25 March and 18 May 2013 at SASP (Skiles, 2014). The details of this validation effort are largely outside the scope of this paper, and here, we briefly summarize that the radiative forcing estimated with SNICAR (dust impact only) was, on average, 25 W m^{-2} less than reported radiative forcing estimated with the Painter method (dust+grain growth). This difference is similar to the portion of radiative forcing accounted for by grain growth in the Painter method over the same time period (24 W m^{-2}). This difference is also similar in magnitude to the overall flux error (-20 W m^{-2}) attributed to SNICAR at SASP that is because of albedo modelling errors (Skiles, 2014). These physically based results lend confidence to the semi-empirical radiative forcing values reported here. We refer the reader to chapters 2–4 of Skiles, 2014 for the full description of the validation.

Snowmelt. The snow energy balance model, SNOBAL, was used to model snowmelt at each of the sites (Marks and Dozier, 1992; Marks and Dozier, 1992). The model represents the snow pack as two layers: an active 25 cm first layer and then remainder of the snowpack as the second layer. Energy exchanges are calculated in the active upper layer, and then energy transfer is determined for the snowpack as a whole, from which the energy available for phase changes in both layers is determined. The model utilizes site elevation, measurement heights, roughness length, and initial snow state variables (snow depth, snow density, snow surface temperature, average snowpack temperature, and liquid water content) as starting inputs. The starting snowpack conditions, or initial state variables, are determined from the manual snow measurements performed closest in time to April 15 (the date of average peak snow for the region) at each site. Changes in state variables, updated at an hourly time step, are driven by the observed forcing variables measured at each site (hourly averages of net shortwave, longwave irradiance, air temperature, relative humidity, wind speed, and precipitation mass). The dust-laden snowpack is modelled from tower measurements, representing observed dust in snow conditions. The clean snowpack is modelled by removing the minimum and maximum radiative forcing due to dust from the measured net shortwave, followed by averaging the daily values of these two scenarios.

A detailed description of SNOBAL can be found in Marks *et al.* (1998). An extended discussion of how SNOBAL is applied to assess how dust advances snowmelt, as well as a model sensitivity study completed using SBBSA instrumentation accuracy ranges, can be found in Skiles *et al.* (2012). Briefly, the largest uncertainties are associated with longwave irradiance, net solar radiation, and wind speed measurements with 1–2 days difference in melt-out date. The maximum uncertainty is 2–3 days for all combined uncertainty ranges (+,–). The model surface roughness parameter was also assessed, as this value is set to a constant (1 mm). It was found that the SNOBAL is not highly sensitive to alterations in this parameter until the values were increased beyond what was physically reasonable at these sites (5 cm). Overall, SNOBAL effectively models the evolution of snowpack, consistently melting out snow cover to within a day of observed SAG across all years.

RESULTS AND DISCUSSION

Measurements

Energy balance and snow cover. Sites GMSP and SASP are very similar with respect to meteorological and radiation fluxes from 2010 to 2013 (Figure 2). Both sites exhibit similar mean relative humidity (60%) and mean temperatures. The GMSP site is, on average, 0.3 °C warmer than SASP. The GMSP and SASP sites both have mean maximum summertime temperatures of 20 °C and mean minimum wintertime temperatures of –18 °C. The largest meteorological variation between the two sites is wind speed. Although both sites are well protected and exhibit relatively low yearly average wind speeds (1 m s^{–1} at SASP, 2 m s^{–1} GMSP), wind speeds are consistently higher at GMSP. Over the full year, GMSP averages 1 m s^{–1} windier than SASP, and hourly wind speeds can reach 10 m s^{–1} at GMSP, while they do not exceed 5 m s^{–1} at SASP. Radiation fluxes are slightly higher at GMSP, as on average there is 8 W m^{–2} greater solar contribution and 6 W m^{–2} thermal contribution (longwave) at GMSP than SASP. This condition could be due to stronger shadowing effects at the SASP site related to its mountainous terrain.

The accumulation and duration of snow cover are controlled by these fluxes. Snow typically begins to accumulate at both sites in November as solar irradiance decreases and temperatures decline. Snow cover reaches a maximum depth in March or April and then decreases with increasing solar irradiance to SAG in May or June. Both sites have similar snow accumulation and ablation patterns, with 1.0 m average seasonal snow depths. Nevertheless, the date of maximum snow depth, marking the transition between snow accumulation and ablation,

typically occurred later at GMSP. In 2011 and 2012, this difference was only one day, but in 2012, it was by 12 days, and in 2013, it was nearly 40 days. Although there was not much more snow at site GMSP in 2013, on average, only 10 cm more than that at SASP, snow accumulation peaked higher and lasted longer at GMSP.

Ablation season coincides with the seasonal increase of solar irradiance in the spring, because among the snow energy balance terms, net solar flux contributes the most energy towards driving snowmelt (Marks and Dozier, 1992; Oerlemans, 2000). In Figure 3, we show broadband, NIR/SWIR, and visible albedo over the ablation season for each site. The reflected flux has been corrected for slope and aspect following the method described in Painter *et al.* (2012). Increases in albedo over this time period were due to new snowfall, and sharp decreases were due to absorption by dust being at or near the snow surface and ensuing feedbacks. In the absence of new snowfall, snow albedo will always gradually decrease over time because of grain growth and increased NIR absorption, at these sites dust is always present in the spring and dominates albedo decay patterns. The albedos at GMSP and SASP co-vary closely with each other; this relation indicates that dust and new snowfall events occur at each site coincidentally, as observed in snow stratigraphy (Figure 4).

Dust deposition. Since 2003, a total of 87 dust events coincident with snow were recorded in SBBSA. Dust-deposition events are not evenly distributed over the record (Figure 5). The number of events increased from 3 in 2003 to 12 in 2009. From 2009–2013, the number of events varied between 9 and 12. Dust events were not distributed evenly across the snow-covered season, as 80% of them occur in March, April, and May (Figure 5). This pattern was related to coincidence of the springtime aridity and atmospheric momentum exchange.

The timing of dust deposition is important for the radiative impact. Dust deposited in winter is usually buried by additional snow, thus limiting the duration of absorption of additional solar radiation at the surface. In contrast, dust deposited in the spring has the largest impact on melting, because solar irradiance is increasing and the internal energy in the pack is great enough to initiate snowmelt. Additionally, dust remains in the layer in which it was deposited and is not entrained in melt water, a process that results in newly deposited spring dust layers persisting at the surface and previously buried layers resurfacing and converging as snow cover diminishes. Such coalescence of layers further darkens the surface and compounds albedo decay. The stationary behaviour of dust layers as snow melts has been consistently observed at SBBSA (Painter *et al.*, 2012) and has also been reported for light absorbing impurities in other regions (Conway *et al.*, 1996; Doherty *et al.*, 2013).

DUST-ON-SNOW SPATIAL VARIABILITY

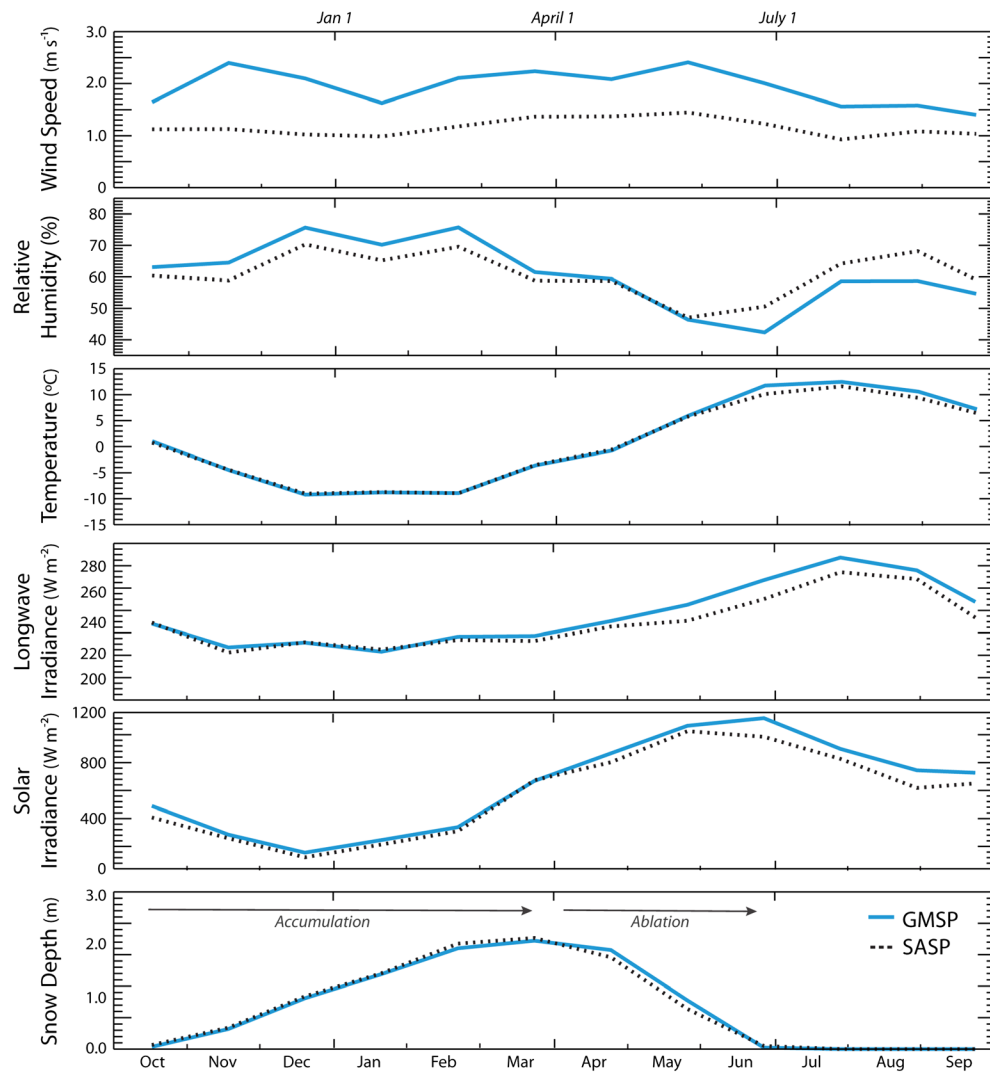


Figure 2. Monthly mean (2010–2013) instrumentation tower measurements at Swamp Angel Study Plot (SASP) (black dotted line) and Grand Mesa Study Plot (GMSP) (blue line). Wind speeds are slightly higher at GMSP; otherwise, the two sites are climatologically very similar, particularly during snow-covered months

Dust concentrations. The amount of dust entrained during each event was variable. Therefore, the number of events each season was not a predictor of the amount of dust deposited each season (Figure 6). Moreover, end-of-year (EOY) dust concentrations exhibited greater interannual variability than number of seasonal dust events (Figure 5). The season total dust concentrations reported here are the values from last collection of the season. These EOY samples were collected just prior to snow depletion when all dust was combined at the surface. In this study, additional dust was not deposited during the time between the last sample collection and SAG.

The heaviest dust deposition and widest range of dust concentrations occurred at SASP. Between 2010 and 2013, EOY concentrations ranged from 0.83 mg g^{-1} in 2012 to 4.80 mg g^{-1} in 2013, with an average concentra-

tion of 2.82 mg g^{-1} . Over the full record (2005–2013), the range was 0.22 mg g^{-1} (2005) to 4.80 mg g^{-1} (2013) with a median and average concentrations of 0.99 mg g^{-1} (2006) and 2.09 mg g^{-1} , respectively. The EOY concentration distribution exhibited two modes: extreme dust years (2009, 2010, and 2013) where the loading was greater than 4.0 mg g^{-1} and lower dust years (2005–2008 and 2011–2012) where the loading was $\sim 1.0 \text{ mg g}^{-1}$ or less. Note, here we discuss dust concentration, the amount of dust relative to the amount of snow in each sample, and not column dust loading, the amount of dust per unit area, but the relation between the two is linear (Figure 8; $R^2 = 0.99$).

At GMSP, EOY dust concentrations were consistently lower but still exhibited distinct interannual variability, albeit with a narrower range of values. Concentrations ranged from 0.6 mg g^{-1} in 2012 to 1.65 mg g^{-1} in 2010,

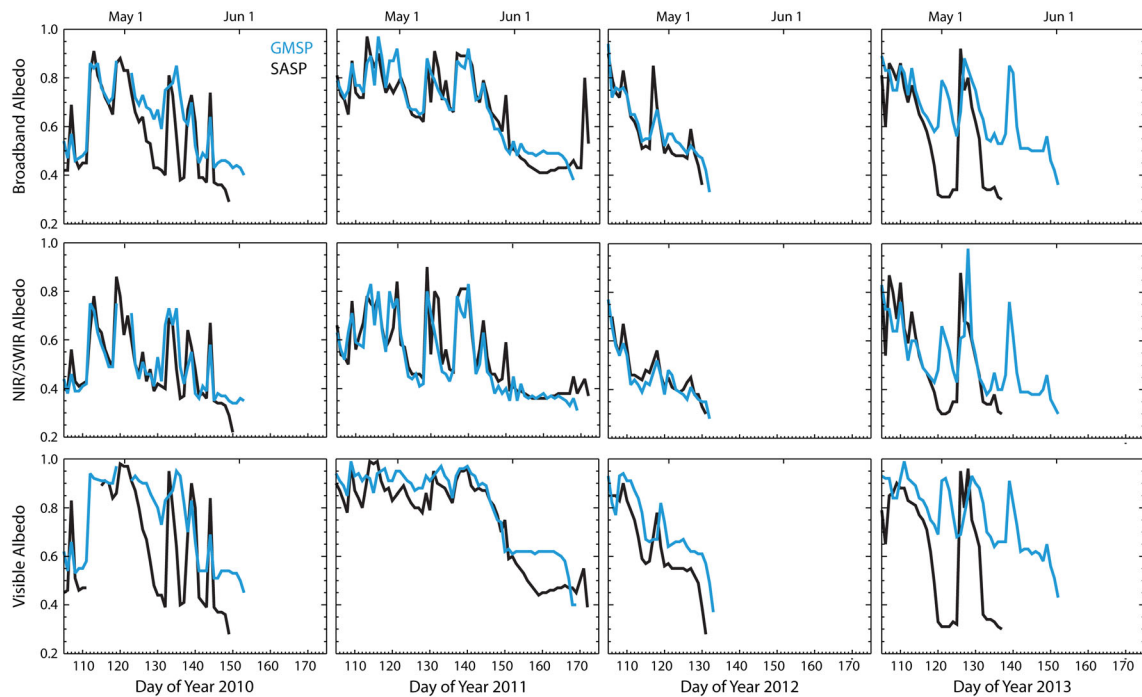


Figure 3. Broadband, NIR/SWIR, and visible snow albedo at Swamp Angel Study Plot (SASP) (black lines) and Grand Mesa Study Plot (GMSP) (blue lines), plotted from 15 April to snow all gone. Albedo is the ratio of incoming to outgoing solar radiation, as measured at the towers. With a few exceptions, the reflectance at the sites shows positive covariance, indicating the timing if new snowfall, dust deposition, and dust emergence is approximately coincident between sites

with an average concentration of 1.0 mg g^{-1} . On average, the concentrations at GMSP were 1.1 mg g^{-1} lower than those at SASP. The site-to-site difference was the smallest, 0.24 mg g^{-1} , in 2012, the lowest dust year at both sites over the coincident record. The difference was potentially the largest, $\sim 4 \text{ mg g}^{-1}$, in 2013, the highest dust year on record at SASP. We cannot be certain of this absolute value because the 2013 GMSP, EOY concentration was estimated, as described in the succeeding discussions. It is not unreasonable, though, to suggest that the largest difference in dust loading between the two sites occurred in 2013, as albedo changes were not as drastic and the snow cover lasted much longer at GMSP than at SASP.

Note that due to the slightly higher wind speeds at GMSP, dust-deposition patterns can exhibit more site-scale variability than at SASP, and therefore, there is higher uncertainty associated with GMSP measurements and how representative they are. The few comparisons we have been able to make between samples collected by CSAS and SOL, within a few days of each other at different study plot locations, indicates that the variability within study plot boundaries is $\sim 0.1 \text{ mg g}^{-1}$, which is a 6–20% uncertainty relative to the range of end of year dust concentrations. A longer record will allow us to assess this in greater detail.

Although an EOY gravimetric sample was not collected at GMSP in 2013, a bulk sample was collected

near the site on 21 May 2013 for USGS analysis. We were able to use this to estimate the 2013 EOY dust concentration because of (1) the linear relation between EOY dust concentrations and dust loading from gravimetric sampling (Figure 7) and (2) the relatively small difference between loading from gravimetrics and those from bulk samples (approximately $\pm 1 \text{ g m}^{-2}$ across all years that have corresponding samples). Typically, bulk samples were collected over a 0.5-m^2 area; however, the area sampled during the GMSP collection on 21 May 2013 was not noted. Therefore, we bracketed the potential area of collection with low-area (0.3 m^2), mid-area (0.6 m^2), and high-area (0.9 m^2) end members, based on knowledge of previous sample collections. The total dust mass was 2.8608 g , with corresponding, respective loading estimates of 9.54 , 4.77 , and 3.18 g m^{-2} . Substituting these values into the slope equation ($y = 10.82x - 0.537$) returned dust concentration estimates of 0.83 , 0.39 , and 0.24 mg g^{-1} for the low-area, mid-area, and high-area end members, respectively, with a $\pm 0.1 \text{ mg g}^{-1}$ uncertainty due to the variation in loading between bulk and gravimetric samples.

We adopted the low-area end member concentration ($0.83 \pm 0.1 \text{ mg g}^{-1}$) as our best estimate of EOY dust concentrations at GMSP in 2013 based on the linear relationship between EOY dust concentrations and dust advanced melt (Skiles *et al.*, 2012), discussed further in Advanced snowmelt section.

DUST-ON-SNOW SPATIAL VARIABILITY



Figure 4. Photographs of the upper ~50 cm of two snow pits at Swamp Angel Study Plot (SASP) and Grand Mesa Study Plot (GMSP) in early May 2010. While dust loading is typically lower at GMSP, the two pits exhibit similar dust stratigraphy indicating coincident dust event timing (regular observations of dust events occur only at SBBSA). Note the new snowfall seen at SASP had undergone densification/melt by the time snow sampling occurred at GMSP

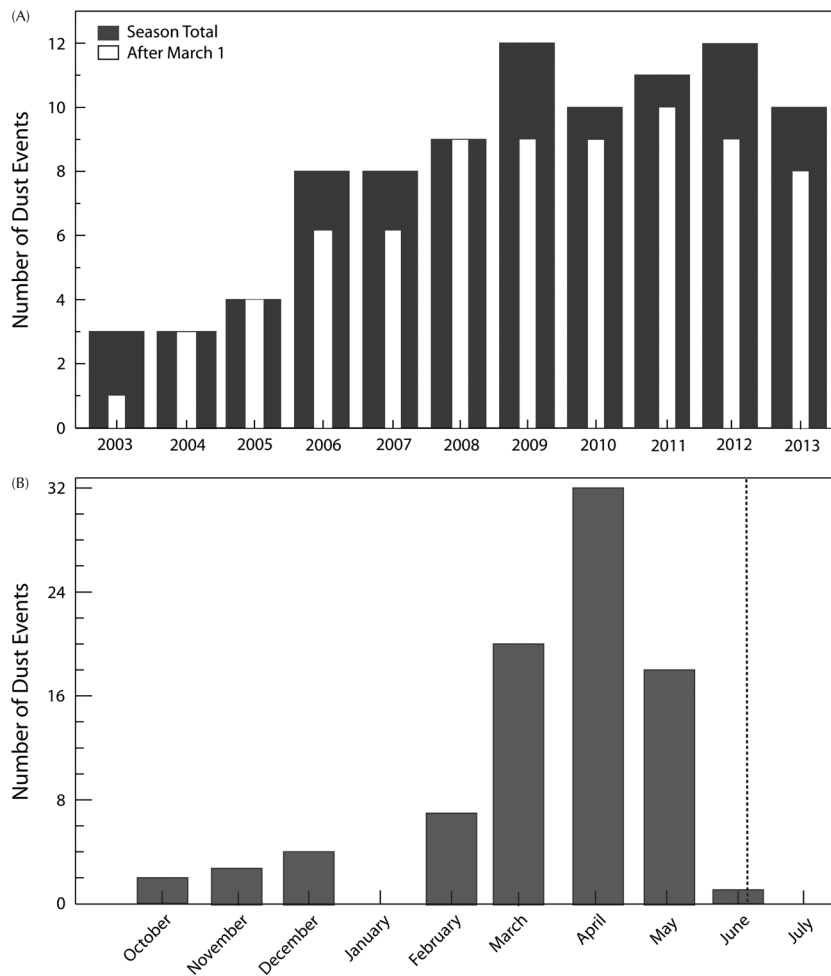


Figure 5. Dust events at Senator Beck Basin Study Area over the full record of observation. (A) The number of events for each season, as well as how many of those events occurred in the spring. (B) The monthly distribution of events, with basin average snow all gone date indicated by the dotted line

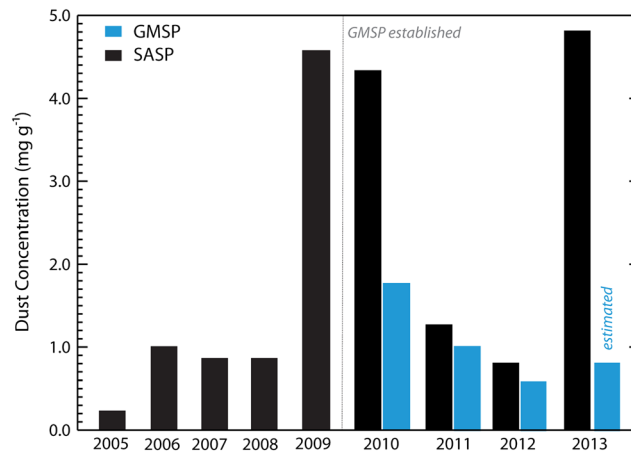


Figure 6. End of year dust concentrations for Swamp Angel Study Plot (SASP) (2005–2013) and Grand Mesa Study Plot (GMSP) (2010–2013). An end-of-year gravimetric sample was not collected at GMSP in 2013, and ranges of concentrations were estimated from dust loading. Here, we show the highest estimate, which was adopted due to the linear relationship between end of year dust concentrations and dust advanced melt (Advanced snowmelt section, Figure 12)

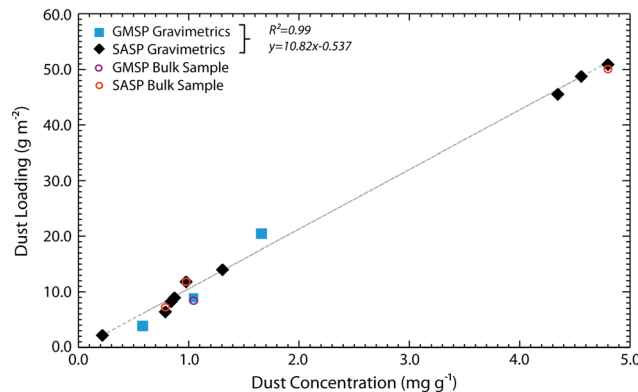


Figure 7. The relation between end of year (EOY) dust loading and dust concentration from gravimetric sampling. These are taken from the last sample collection of the season, when individual dust event layers have coalesced at the surface, and represent season total dust loading. Corresponding dust loading from EOY bulk samples are within $\pm 1 \text{ g m}^{-2}$ of those from gravimetric samples, which indicates that dust loading from bulk samples could be used to approximate dust concentrations in the absence of gravimetric sample collection, as we did for GMSP EOY 2013. GMSP, Grand Mesa Study Plot; SASP, Swamp Angel Study Plot

The relatively high interannual variability in dust loading can be generally ascribed to surface dynamics in the source regions and synoptic meteorology. The details of these factors are beyond the scope of this paper. A recent study by *Li et al.* (2013) found a relation between the amount of bare ground, as identified from remote sensing imagery, and dust loading at SBBSA. *Flagg et al.* [2013] measured emission in southeastern Utah between 2003 and 2012 and found wind speeds to be the strongest predictor of dust flux, with the strong spring-time winds across the Colorado Plateau producing the highest fluxes. Other factors, such as vegetation cover/type and soil type, also played a role in emission fluxes (*Flagg et al.*, 2013). Heavy dust-on-snow years cannot likely be attributed to a single factor, and additional study is needed to better understand the relations among source region, atmospheric transport, and deposition processes.

Modelling

Dust source regions. We classified the azimuthal directions of each footprint (Table I) and plotted representative events for these classifications (Figure 8). The majority of spring-time events were classified as extending to the southwest. Relative to SBBSA footprints, GMSP footprints were northerly and more westerly. The potential source regions are most similar for the two sites when footprints extend to the south and are most divergent when footprints extend to the west in trajectories latitudinal to the sites. No footprints extend directly to the north or east for either of the study areas. Full season averages (Figure 8) approximate the general southwest direction of the individual events. An exception is found for 2013, when individual events and the seasonal average were more westerly than the other years. This observation may be

DUST-ON-SNOW SPATIAL VARIABILITY

Table I. Summary of spring dust event timing, event dust loading at Swamp Angel Study Plot (from Center For Snow and Avalanche Studies), modelled source area, and observed source region (from United States Geological Survey) when available for 2010–2013. If dust events were uniquely sampled, dust loading is noted. If dust events were deposited when dust was already at the surface, visual event identification is noted. These observations are not available for 2010. Events that took place after snow-all-gone at either site are not listed

Event date	Event #	Dust loading (g m ⁻²) dust loading (g m ⁻²)	Visual identification	Source region	Observed source
<i>2010</i>					
30 Mar	D2			<i>SBBSA</i> SW	<i>GMSP</i> SW NE AZ
3 Apr	D3			W/SW	W/NW —
5 Apr	D4			SW	W/SW NE AZ, NW NM
12 Apr	D5			S	S NE AZ, NW NM
28 Apr	D6			SW	SW NE AZ, NW NM
9 May	D7			SW	SW —
11 May	D8			SW	W/SW NE AZ, NW NM
22 May	D9			SW	SW AZ,NM
<i>2011</i>					
17 Mar	D3	0.14		SW	W/SW —
21 Mar	D4	2.56		S	S —
8 Apr	D5	0.61		SW	SW —
21 Apr	D6	0.34		SW	SW —
29 Apr	D7	0.24		SW	W —
9 May	D8	0.54		SW	SW —
18 May	D9		Minor event	SW	SW —
26 May	D10		Minor event	W/SW	W —
29 May	D11		Major event	SW	SW NE AZ, NW NM
<i>2012</i>					
18 Mar	D5	1.64		S	S —
26 Mar	D6		Minor event	S	S NE AZ, NW NM
1 Apr	D7		—	SW	SW —
6 Apr	D8		Major event	SW	SW —
<i>2013</i>					
17–18 Mar	D4	0.20		W	W
21–22 Mar	D5	0.60		W/SW	W
8 Apr	D6	23.73		SW	W
13–14 Apr	D7	1.60		W/SW	W
15–17 Apr	D8	4.58		SW	W/SW
30 Apr	D9		Minor event	W	W

related to the three events in 2013 that were reported as multi-day events, resulting in broader footprint extents.

Dust loading at SASP was compared with back-trajectory footprints for the same events. At SASP, we sampled 12 individual spring-time events between 2011 and 2013. Dust loading ranged from 0.28 g m⁻² (17 March 2011) to 47.46 g m⁻² (8 April 2013) with a median value of 1.22 g m⁻² (8 April 2011) (Table I). These comparisons revealed that south and southwesterly events tended to deposit the most dust, though not every southwesterly event brought heavy dust loading. Note that when dust events were observable from remote sensing images, the identified sources were consistently to the south/southwest of SASP in northwestern New Mexico and/or northeastern Arizona, and correspondingly, the SASP footprints were south/southwest for these days.

The heaviest single-event dust load was associated with the 8 April 2013 (D6) event. The D6 event deposited a

dust mass that accounted for more than 90% of the total dust mass in 2013 and more dust than was deposited across all other seasons. We currently have no knowledge of the factors that forced this uniquely large event. The back-trajectory footprint, shown in Figure 9, is west to southwest, spatially broader than the relatively more constrained footprints exhibited by other major events. The footprint for GMSP was distinctly more northerly for this event, and the albedo record and longer duration of snow cover at GSMP in 2013 suggested that the dust loading was not as heavy.

The differences in dust loading at sites SASP and SBBSA in the SJM vis-à-vis site GMSP likely arise from a combination of several physiographic, meteorological, and geomorphic, including soil, factors. Certainly, these sites have common source areas under some wind conditions (e.g. ‘south’ back trajectories in Figure 8) especially as wind storms track from west to east.

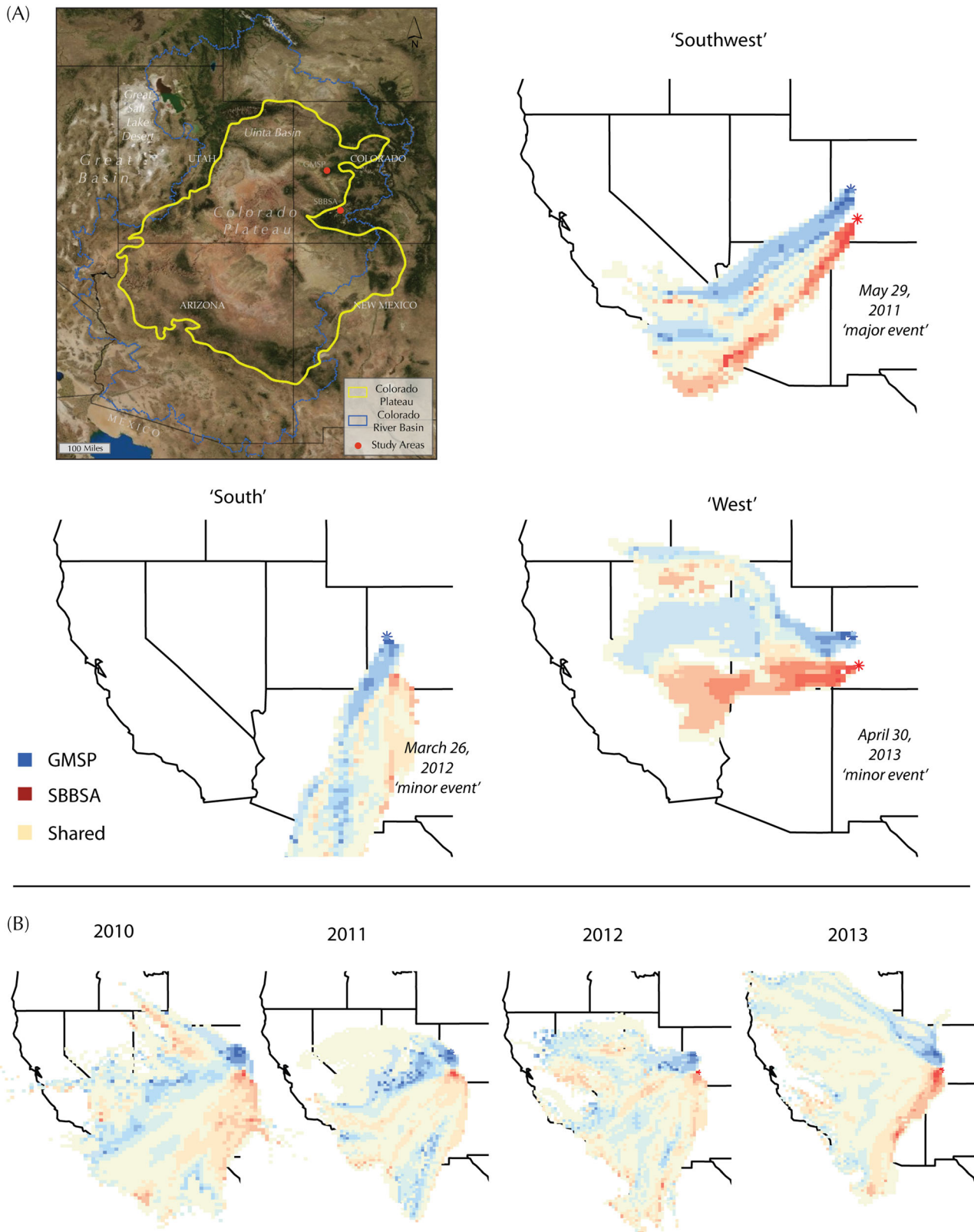


Figure 8. (A) 24-h back-trajectory footprints that are representative of trajectory classifications from table I. (B) 24-h back-trajectory averages of each year's springtime events. All plots represent footprint differences; where beige is the area GMSP and SBBSA have in common, blue is GMSP only, and red is SBBSA only. The colours are most intense both where there are more particles and where footprints are most unique. For reference, we show a map of the western USA with relevant geographic regions outlined or labelled. GMSP, Grand Mesa Study Plot; SBBSA, Senator Beck Basin Study Area.

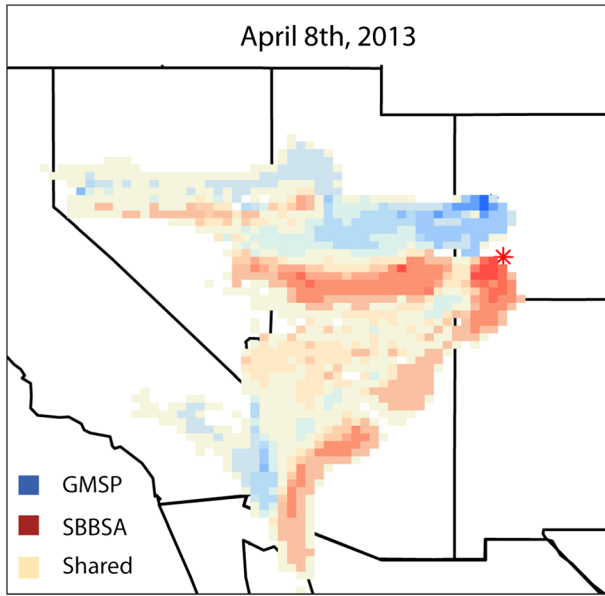


Figure 9. The 24-h back-trajectory for 8 April 2013, the single largest dust event recorded since 2005; blue denotes trajectories for GMSP only, red for SBBSA only, and beige for a common source region. GMSP, Grand Mesa Study Plot; SBBSA, Senator Beck Basin Study Area

Nevertheless, the back-trajectory patterns can be distinct for individual events and for annual averages (Figure 8). With respect to events, we note that (1) the ‘southwest’ May 2011 back trajectories for site GMSP are more northwesterly than those for SASP, (2) the ‘south’ March 2012 back trajectories for site GMSP are more westerly, and (3) the ‘west’ April 2013 back trajectories for site GMSP are more northerly. Although with broad overlap on yearly averages, dust sources for SJM are dominantly southerly and southwesterly (Figure 8), whereas those for GSMP are dominantly westerly and northwesterly.

Modelling and satellite-retrieval observations have already revealed that sources for dust deposited to the SJM are commonly from the southern Colorado Plateau (Painter *et al.*, 2007; Neff *et al.*, 2008; Lawrence *et al.*, 2010). Sometimes, large and distinct dust plumes produced from many different types of geomorphic surfaces have been observed passing close to and across the Four Corners region en route to SJM (http://sgst.wr.usgs.gov/dust_detection/dust-events/). These sources are numerous and widespread across mostly flat – that is, topographically uninterrupted – expanses having long wind fetch to the southwest. In addition, some of the dust sources there occur in long, broad, and un-entrenched drainage systems oriented SW-NE. Thus, southwesterly winds sweep parallel to the long dimension, high fetch of these systems that are filled with fine-grained sediments derived from easily erodible sedimentary rocks. Sand dunes and dune fields reflect the dominant southwesterly strong-wind orientation. Other sources, though, such as dry lake surfaces, have no such orientation.

The back trajectories for site GMSP commonly cross landscapes of benches and mesas, cut by canyons, as on the central Colorado Plateau, as well valleys and mountains of the high-relief eastern Great Basin Desert. Notably, the basins and ranges of the Great Basin Desert are mostly oriented north–south. Moreover, some westerly and northwesterly back trajectories for site GMSP cross the Great Salt Lake Desert and Uinta Basin in northern Utah. In the eastern Great Basin Desert, modern and late Quaternary lake-bed surfaces and alluvial deposits produce dust from both natural and disturbed settings. Recently, parts of the Uinta Basin have undergone extensive development and surface disturbances related to fossil–fuel extraction. More details about dust emission and wind in the Great Basin Desert are provided by Schafer and Steenburgh (2008), Reynolds *et al.* (2010), Jewell and Nicoll (2011), Steenburgh *et al.* (2012), Miller *et al.* (2012), Hahnenberger and Nicoll (2012; 2014).

In light of the foregoing observations, it appears that dust-source settings on the southern Colorado Plateau differ generally from those that produce dust captured at site GMSP. On the basis of surveillance and regional topography, the sources sending dust primarily to SJM may overall be more exposed to strongest winds, and (or) are larger in total area, and (or) are more numerous. These and other possibilities, such as soil-moisture conditions and topographic focusing or deflectance of dust-bearing winds, are worthy of detailed investigation.

Radiative forcing. Dust radiative forcing is typically initiated in March with the deposition of springtime dust events and increased over the ablation season with additional dust deposition and snow albedo feedbacks. To capture this rise in spring radiative forcing, we calculate it for each year from March 15 to the date of modelled clean SAG (Figure 10). Spring radiative forcing is controlled by the amount of dust at, or near, the snow surface and is modulated by new snowfall. Although a number of cloudy days presumably would decrease dust radiative forcing by reducing incoming solar irradiance, Skiles *et al.* [2012] found no relations between cumulative broadband irradiance and daily mean radiative forcing at SBBSA. Temporal relations among daily means radiative forcing along with precipitation, snow depth, and dust events are shown in Figure 10.

Radiative forcing from April 15 to observed date of SAG indicates the contribution of dust to melting energy over the ablation season. The highest daily mean values consistently occurred at the SASP site, which received the most dust. Between 2010 and 2013, the highest and lowest daily mean radiative forcing occurred in 2013 (65 W m^{-2}) and 2012 (50 W m^{-2}), respectively, corresponding to the highest and lowest EOY dust concentrations. Over the full record, the highest mean radiative

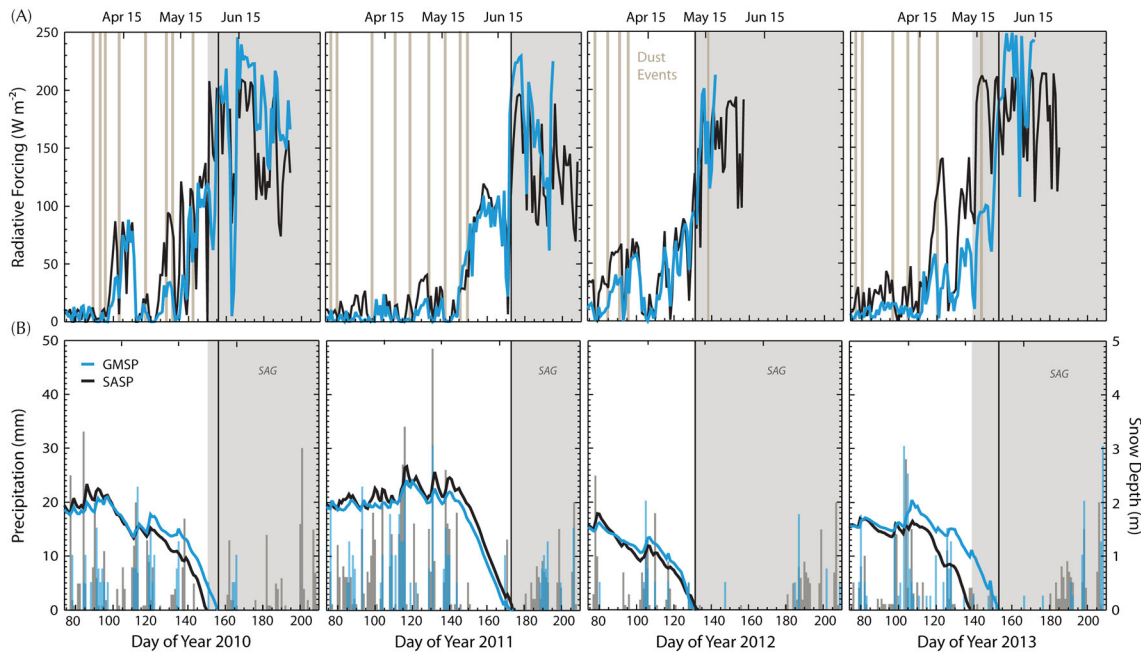


Figure 10. (A) Dust radiative forcing and observed dust-event timing and (B) observed snow-cover depth and precipitation, plotted from 15 March at SASP and GMSP. The grey shading indicates snow all gone (SAG) at Swamp Angel Study Plot (SASP), and the solid black vertical line represents the SAG date at Grand Mesa Study Plot (GMSP)

forcing occurred in 2009 (75 W m^{-2}), the second highest dust concentration year, and the lowest ablation season radiative forcing (35 W m^{-2}) occurred in 2005, the lowest dust concentration year (Skiles *et al.*, 2012).

Similar evolution in radiative forcing is exhibited at GMSP compared with SASP but having lower magnitude. The highest daily mean radiative forcing occurred in 2010 (50 W m^{-2}), and the lowest was in 2012 (35 W m^{-2}), values which were also associated with the highest and lowest EOY dust concentrations measured at GMSP. While the record high dust deposition at SASP occurred 2013, our EOY dust concentration estimation and these radiative forcing values would indicate that 2010 was the heaviest dust year GMSP, as ablation season radiative forcing in 2013 (39 W m^{-2}) was lower than in 2010 (50 W m^{-2}). Across all years, daily mean radiative forcing was 16 W m^{-2} less than that at SASP.

Mean daily radiative forcing from April 15 to clean-scenario SAG provides an encompassing measure of dust-forced-snow-albedo feedbacks, including enhanced grain growth and earlier removal of snow cover. The daily mean radiative forcing over this period was highest in 2013 at both sites, with 130 W m^{-2} at the SASP and 95 W m^{-2} at GMSP. Average values for the SASP and GMSP were 105 W m^{-2} and 88 W m^{-2} , respectively. At both sites, an additional $28\text{--}65 \text{ W m}^{-2}$ of radiative forcing was found for the period of April 15 to clean-scenario SAG relative to dust-scenario SAG. This additional forcing came from the earlier reduction in snow cover, as radiative forcing after observed SAG represents the

difference in absorption between snow and the darker underlying substrate.

Advanced snowmelt. The additional energy contribution from dust radiative forcing contributes to earlier snowmelt (1) by reducing cold content of the snow column when snow temperature is $<0^\circ\text{C}$ and (2) by supplying energy towards melt when snow temperature is at 0°C (Painter *et al.*, 2012; Skiles *et al.*, 2012). As discussed in the Methods section, the clean snowpack was modelled by removing the minimum and maximum radiative forcing due to dust, and then averaging the daily values of these two scenarios to represent a conservatively clean snowpack. Without direct observation of zero-dust conditions, the modelled clean-snow scenario represents our best understanding of the evolution of the snowpack in the absence of dust. We refer to the difference in the number of days between the SAG dates of the dust and clean scenarios as ΔSAG . Evolution in SWE over the ablation season is plotted in Figure 11.

The capacity of the snowmelt model to reconstruct accurately snow cover can be assessed by comparing measured with modelled SWE for observed conditions, i. e. the dust scenario (Figure 11). The root mean square difference of modelled to measured SWE over the ablation season at SASP is 49 mm across all years (51 measurements; 2005–2013). Because of sparse measurements of ablation-season SWE at GMSP, we did not calculate RMSDs there. Nevertheless, the modelled SAG

DUST-ON-SNOW SPATIAL VARIABILITY

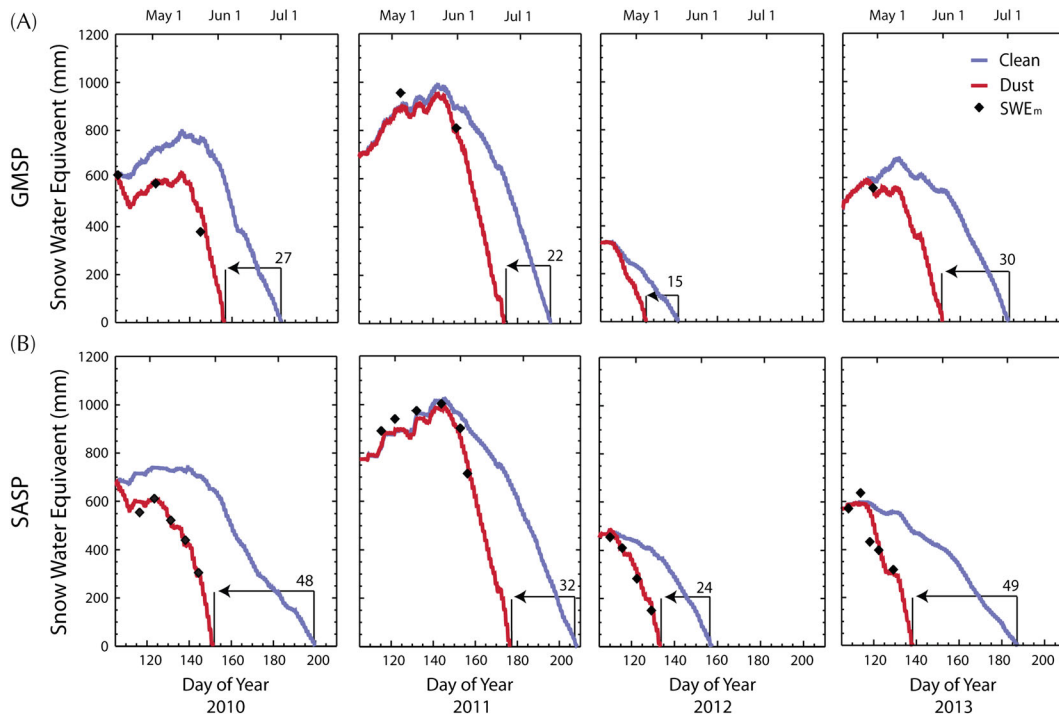


Figure 11. Depletion of snow water equivalent (SWE) plotted from 15 April, at (A) Grand Mesa Study Plot (GMSP) and (B) Swamp Angel Study Plot (SASP), with days of advanced melt because of dust (Δ SAG) indicated. The red line (modelled SWE under observed conditions) matches well with measured SWE (black diamonds), indicating the model does a good job of reconstructing of snowmelt

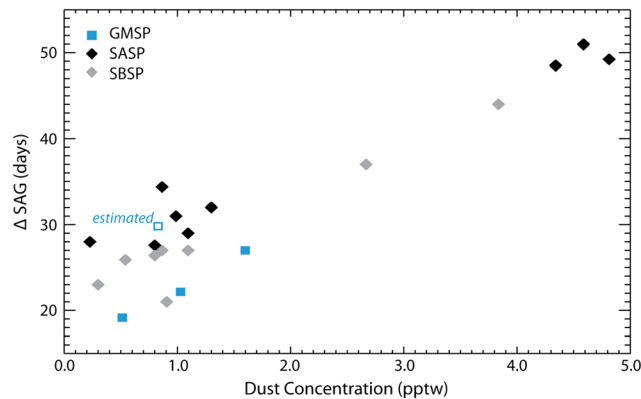


Figure 12. The relation between end-of-year dust concentration and the number of days by which dust advanced snowmelt at each site for 2005–2013 at Swamp Angel Study Plot (SASP), 2005–2012 at Senator Beck Basin Study Area (SBSP), and 2010–2013 at Grand Mesa Study Plot (GMSP). We include SBSP here to show a similar linear response to dust radiative forcing at all sites. A range of potential end of year (EOY) dust concentrations were estimated from EOY dust loading at GMSP in 2013, and given the degree of advanced melt in 2013, the highest estimate (shown here) is the most probable concentration

occurred within 1 day of observed SAG, which is determined from the snow depth sensor, across all 4 years, thereby giving confidence that the model adequately simulates snow cover at this site.

Radiative forcing by dust varies on multiple temporal scales, and degree to which it advances snowmelt can be influenced by factors such as the amount of SWE the ground at the beginning of the ablation season (Painter *et al.*, 2007), the amount of new snow fall atop dust layers

in the spring (Skiles *et al.*, 2012), and the variation in solar irradiance by cloud cover (Skiles *et al.*, 2012). We find that the effects of these tempering factors do not influence the linear relationship we find between Δ SAG and end-of-year dust concentrations exhibited at SBBSA over the full 9-year record (Figure 12; R^2 value of 0.95).

A similar linear Δ SAG response to EOY dust concentrations is exhibited at GMSP (Figure 12). Over the 3 years with measured dust loading, 2010 had the

greatest advanced melt (27 days), and 2012 had the lowest (15 days). The Δ SAG value was higher in 2013 than in 2010, but the estimated dust concentration in 2013 was lower. Because the data for 2013 were generated from relatively few observations, we consider the estimate for the 2013 EOY dust concentration to be very rough. A longer record at GMSP would help us better understand variability at this site.

CONCLUDING THOUGHTS

Dust deposition at GMSP between 2010 and 2013 resulted in daily mean radiative forcings of $35\text{--}50\text{ W m}^{-2}$ advancing melt by 15–30 days. Dust deposition at SASP over the same time period resulted in daily mean radiative forcings of $50\text{ to }65\text{ W m}^{-2}$, advancing melt by 24–49 days. Whereas evidence suggests that timing of dust events is roughly coincident between the two sites, the dust loading at GMSP is on average $\sim 1\text{ mg g}^{-1}$ less than that at SASP. The relatively low dust concentrations and daily mean radiative forcings at GMSP imply that the degree of dust influence across the CRB may not be as extreme as that attributed to SBBSA. In any case, GMSP exhibits a similar snowmelt response to dust, and dust deposition at GMSP has a very large effect on snow melt in this part of the Upper CRB, accelerating snowmelt there by 24 days on average.

Although previous work has investigated interannual variability in dust loading, radiative forcing, and snowmelt rates, spatial variability in these processes in the CRB is still not well understood. Moreover, data are sparse on dust emission timing and variability from potential source areas (Flagg *et al.*, 2013). This work contributes to the growing body of literature on dust-source regions, dust-on-snow loading, and dust radiative forcing in the western United States. Increasingly, we are improving our understanding about how dust-on-snow deposition affects runoff quality and quantity in the Upper CRB. This line of investigation is important for water security, given the heavy demand on the river system, and given that heavy dust loading will likely become more frequent in future years as expected warming may create deeper and longer droughts, reduce plant cover, and increase dust emissions (Seager *et al.*, 2007; Munson *et al.*, 2011; Li *et al.*, 2013).

ACKNOWLEDGEMENTS

We acknowledge Chris Landry/The Center for Snow and Avalanche Studies for data retrieval, compilation, and availability. We would like to thank three anonymous reviewers for their constructive comments, which improved this manuscript. This work was funded by the

NASA project NNX10AO97G and JB received funding from the USGS Ecosystems and Climate and Land Use programmes. Part of this work was performed at the Jet Propulsion Laboratory, California Institute of Technology under a contract from NASA. Any use of trade names is for descriptive purposes only and does not imply endorsement by the U.S. Government.

REFERENCES

- Belnap J, Gillette D. 1998. Vulnerability of desert biological soil crusts to wind erosion: the influences of crust development, soil texture, and disturbance. *Journal of Arid Environments* **39**: 133–142.
- Brahney J, Ballantyne AP, Sievers C, Neff JC. 2013. Increasing Ca²⁺ deposition in the western US: the role of mineral aerosols. *Aeolian Research* **10**: 77–87. DOI:10.1016/j.aeolia.2013.04.003.
- Bryant J, Painter TH, Deems J, Bender SM. 2013. Hydrologic response to dust radiative forcing in snow in the Upper Colorado River Basin. *Geophysical Research Letters* **40**. DOI:10.1002/grl.50773.
- Christensen NS, Wood AW, Lettenmaier DP, Palmer RN. 2004. Effects of climate change on the hydrology and water resources of the Colorado River Basin. *Journal of Hydroclimatology* **62**: 337–363.
- Conway H, Gades A, Raymond CF. 1996. Albedo of dirty snow during conditions of melt. *Water Resources Research* **32**: 1713–1718.
- Deems J, Painter TH, Barsugli J, Belnap J, Udall B. 2013. Combined impacts of current and future dust deposition and regional warming on Colorado River Basin snow dynamics and hydrology. *Hydrology and Earth System Sciences* **17**. DOI:10.5194/hess-17-4401-2013.
- Doherty SJ, Grenfell TC, Forsstrom S, Hegg D, Brandt RE, Warren S. 2013. Observed vertical redistribution of black carbon and other insoluble light-absorbing particles in melting snow. *Journal of Geophysical Research, [Atmospheres]* **118**. DOI:10.1002/jgrd.50235.
- Flagg CB, Neff JC, Reynolds RL, Belnap J. 2013. Spatial and temporal patterns of dust emissions (2004–2012) in semi-arid landscapes, southeastern Utah, USA. *Aeolian Research* In Press. DOI: 10.1016/j.aeolia.2013.10.002.
- Flanner MG, Zender C. 2005. Snowpack radiative heating: influence on the Tibetan Plateau climate. *Geophysical Research Letters* **32**. DOI:10.1029/2004GL022076.
- Flanner MG, Zender CS, Randerson JT, Rasch PJ. 2007. Present-day climate forcing and response from black carbon in snow. *Journal of Geophysical Research* **112**. DOI:10.1029/2006JD008003.
- Hahnenberger M, Nicoll K. 2012. Meteorological characteristics of dust storm events in the eastern Great Basin of Utah, U.S.A. *Atmospheric Environment* **60**: 601–612. DOI:10.1016/j.atmosenv.2012.06.029.
- Hahnenberger M, Nicoll K. 2014. Geomorphic and land cover identification of dust sources in the eastern Great Basin of Utah, U.S.A. *Geomorphology* **204**: 657–672.
- Hamlet AF, Mote PW, Clark MP, Lettenmaier DP. 2005. Effects of temperature and precipitation variability on snowpack trends in the western United States. *Journal of Climate* **18**: 4545–4561.
- Jewell PW, Nicoll K. 2011. Wind regimes and aeolian transport in the Great Basin, U.S.A. *Geomorphology* **129**: 1–13.
- Landry C, Buck K, Raleigh MS, Clark MP. 2014. Mountain system monitoring at Senator Beck Basin, San Juan Mountains, Colorado: a new integrative data source to develop and evaluate models snow and hydrologic processes. *Water Resources Research* **50**. DOI:10.1002/2013WR013711.
- Lawrence CR, Painter TH, Landry C, Neff JC. 2010. The contemporary composition of aeolian dust deposited in the San Juan Mountains, Colorado, USA. *Journal of Geophysical Research* **115**. DOI:10.1029/2009JG001077.
- Li J, Okin GS, Skiles SM, Painter TH. 2013. Relating variation of dust on snow to bare soil dynamics in the western United States. *Environmental Research Letters* **8**. DOI:10.1088/1748-9326/8/4/044054.
- Lin JC. 2012. Lagrangian modeling of the atmosphere: an introduction. In *Lagrangian Modeling of the Atmosphere*, Lin JC, Brunner D, Gerbig C,

- Stohl A, Luhar A, Websley P (eds). American Geophysical Union Monographs: 1–11.
- Lin JC, Gerbig C, Wofsy SC, Andrews AE, Daube BC, Davis KJ, Grainger CA. 2003. A near-field tool for simulating the upstream influence of atmospheric observations: the stochastic time-inverted Lagrangian transport (STILT) model. *Journal of Geophysical Research, [Atmospheres]* **108**. DOI:10.1029/2002JD003161.
- Marks D, Dozier J. 1992. Climate and energy exchange at the snow surface in the alpine region of the Sierra Nevada 2. Snow cover energy balance. *Water Resources Research* **28**: 3043–3054.
- Marks D, Kimball J, Tingey D, Link T. 1998. The sensitivity of snowmelt processes to climate conditions and forest cover during rain-on-snow: a case study of the 1996 Pacific Northwest flood. *Hydrological Processes* **12**: 1569–1587.
- Miller ME, Bowker MA, Reynolds RL, Goldstein HL. 2012. Post-fire land treatments and wind erosion – lessons from the Milford Flat Fire, UT, USA. *Aeolian Research* **7**: 29–44. DOI:10.1016/j.aeolia.2012.04.001.
- Munson SM, Belnap J, Okin GS. 2011. Responses of wind erosion to climate-induced vegetation changes on the Colorado Plateau. *PNAS* **108**: 3854–3859. DOI:10.1073/pnas.1014947108.
- Neff JC, Ballantyne AP, Farmer GL, Mahowald NM, Conroy JL, Landry CC, Overpeck JT, Painter TH, Lawrence CR, Reynolds RL. 2008. Increasing Eolian dust deposition in the western United States linked to human activity. *Nature Geoscience* **1**. DOI:10.1038/ngeo133.
- Neff JC, Reynolds RL, Munson SM, Fernandez D, Belnap J. 2013. The role of dust storms in atmospheric particle concentrations at two sites in the western US. *Journal of Geophysical Research* **118**. DOI:10.1002/jgrd.50855.
- Oerlemans J. 2000. Analysis of a 3 year meteorological record from the ablation zone of Morteratschgletscher, Switzerland: energy and mass balance. *Journal of Glaciology* **46**: 571–579.
- Painter TH, Barrett AP, Landry CC, Neff JC, Cassidy MP, Lawrence CR, McBride KE, Farmer GL. 2007. Impact of disturbed desert soils on duration of mountain snow cover. *Geophysical Research Letters* **34**. DOI:10.1029/2007GL030284.
- Painter TH, Deems JS, Belnap J, Udall B, Hamlet AF, Landry CC. 2010. Decreased water yield from the Colorado River Basin under dust-accelerated snowmelt. *PNAS* **107**. DOI:10.1073/pnas.0913139107.
- Painter TH, Bryant A, Skiles SM. 2012. Radiative forcing by light absorbing impurities in snow from MODIS surface reflectance data. *Geophysical Research Letters* **39**. DOI:10.1029/2012GL052457.
- Painter TH, Skiles SM, Deems J, Bryant A, Landry C. 2012. Dust radiative forcing in snow of the Upper Colorado River basin: Part 1. A 6 year record of energy balance, radiation, and dust concentrations. *Water Resources Research* **48**. DOI:10.1029/2012WR011985.
- Reynolds RL, Belnap J, Reheis M, Lamothe P, Luiszer F. 2001. Aeolian dust in Colorado Plateau soils: nutrient inputs and recent change in source. *Proceedings of the National Academy of Sciences* **98**: 7123–7127.
- Reynolds RL, Reheis M, Chaves P, Hinckley T, Tigges R, Clow G, MacKinnon D, Lamothe P, Lancaster N, Miller ME, Yount J, Velasco M, Sides S, Soltesz D, Meeker G, Fulton R, Belnap J. 2003. Dust emission and deposition in the southwestern U.S.—Integrated field, remote sensing, and modeling studies to evaluate response to climatic variability and land use. In *Desertification in the Third Millennium*, Al Sharbon AR, Wood WW, Goudie AS, Fowler A, Abdellatif E (eds). Swets & Zeitlinger: 271–282.
- Reynolds RL, Mordecai JS, Rosenbaum JG, Ketterer ME, Walsh MK, Moser KA. 2010. Compositional changes in sediments of subalpine lakes, Uinta Mountains (Utah): evidence for the effects of human activity on atmospheric dust inputs. *Journal of Paleolimnology* **44**: 161–175. DOI:10.1007/s10933-009-9394-8.
- Schafer JC, Steenburgh WJ. 2008. Climatology of strong intermountain cold fronts. *Monthly Weather Reviews* **136**: 784–807. DOI:10.1175/2007MWR2136.1.
- Seager R, Ting MF, Held I, Kushnir Y, Lu J, Vecchi G, Huang HP, Harnik N, Leetmaa A, Lau NC, Li CH, Velez J, Naik N. 2007. Model projections of an imminent transition to a more arid climate in southwestern North America. *Science* **316**: 1181–1184. DOI:10.1126/science.1139601.
- Skiles SM. 2014. Dust and black carbon radiative forcing controls on snowmelt in the Colorado River basin (doctoral dissertation). In: Geography, University of California-Los Angeles.
- Skiles SM, Painter TH, Deems J, Landry C, Bryant A. 2012. Dust radiative forcing in snow of the Upper Colorado River basin: part II. Interannual variability in radiative forcing and snowmelt rates. *Water Resources Research* **48**. DOI:10.1029/2012WR011986.
- Sorooshian S, Shingler T, Harpold A, Feagles CW, Meixner T, Brooks PD. 2013. Aerosol and precipitation chemistry in the southwestern United States: spatiotemporal trends and interrelationships. *Atmospheric Chemistry and Physics*. DOI:10.5194/acp-13-7361-2013.
- Steenburgh WJ, Massey JD, Painter TH. 2012. Episodic dust events of Utah's Wasatch Front and adjoining region. *Journal of Applied Meteorology and Climatology* **51**: 1654–1669. DOI:10.1175/JAMC-D-12-07.1.